Effect of Target Arrangement and Target Materials Properties on Penetration Depth

T. Sy Ngo, S. Beer and P. Konečný[*]

Faculty of Military Technology, University of Defence in Brno, Czech Republic

Abstract:

The article focuses on the development of the new calculation method of jet penetration into the target using ANSYS AUTODYN simulation. The jet formation and its penetration capability dependence on properties of targets are studied. Two kinds of steel armours - Armox 440T and S235JR – in standardized plates of thickness 20 mm are used as materials of the target. The paper contains an analysis of the penetration depth in the targets containing the pure material plates set, combined material plates set and sets of Armox 440T plates with gaps 10 mm and 20 mm among individual plates. The theoretical results of simulation are compared with the results of experiments.

Keywords:

ANSYS AUTODYN, Eulerian grid, jet formation, Lagrangian grid, penetration – stand-off curve, PG-7V, standoff

1. Introduction

Cumulative ammunition with shaped charge is widely used in armies all over the world to destroy numerous types of targets including tanks and other armoured vehicles. A typical modern shaped charge can penetrate steel armour to a depth measured in the diameters of the charge seven or more times.

Due to the relative independence of the jet penetration from impact velocity, the principle of the shaped charge is extensively used for various antitank ammunition or antitank systems, where the warheads have a relatively simple design. On the other hand, the ammunition does not require a weapon barrel loaded by high pressure, which makes the barrel production easier.

It is known that the jet formation and penetration depth in the target also depend on different parameters, such as the shaped-charge hollow angle α, the liner material

---

[*] *Corresponding author: Department of Weapons and Ammunition, University of Defence in Brno, Kounicova 156/65, CZ-662 10 Brno, Czech Republic. Phone: +420 973 442 037, E-mail: pavel.konecny@unob.cz, ORCID 0000-0003-0703-2315.*

and thickness, the profile of the wave shaper, the density of the main charge, and the standoff distance [1]. The shaped-charge performance is also affected by the manufacturing technology precision, which includes dimensions tolerance, assembly tolerances, etc. [2]. For reaching the maximum penetration depth in the target, one of the most important factors of the shaped charge is the optimal standoff distance of the warhead.

The research of the armours with various properties and structures, as well as their penetration assessment, is permanently topical with respect to the armoured vehicles ballistic resistance to the penetration.

In this article, the target is created from individual armour 20 mm plates. The plate thickness was not chosen. They were used according to cost availability. In addition, the manipulation with such plates was very easy due to their mass.

The main objective is an analysis of variable armour material influence and the influence of gaps between the armour material plates on the shaped charge PG-7V penetration effect that was carried out both theoretically by simulation and experimentally.

2. Materials and Methods

The jet formation theory is very complex. Many authors have published mathematical models capable to predict the penetration of the armour target by the shaped-charge jet. Penetration theories are given in works [2-12]. All of the models are often simplified, and they do not consider the character of materials too much, especially their dynamics character. In addition, heterogeneity in material properties was not mentioned in previous studies.

The Finite Element Model (FEM) was created using ANSYS AUTODYN [13] software, which is widely used in high explosive detonation simulations, high speed impacts, and other problems areas. The software includes its own material library; however, new materials can be added. The new material addition requires density, equations of state, strength models, and other material properties.

2.1. Diagram of Solution

Figs 1-3 show the diagram of solution presented in this article. Based on AUTODYN, the collapse process is built to obtain the velocity and profile of jet, which is shown in Fig. 1. Then, the model was rebuilt using the jet velocity results from the jet formation model to solve the penetration problem in two ways:
- using the gaps between the plates of target,
- using the targets with different materials.

Diagrams of these two cases are shown in Figs 2 and 3, respectively.

2.2. Materials Properties of PG-7V Warhead Parts

For simulation problems in this article, it is necessary to determine the characteristics of the main structural elements (parts), including materials of the PG-7V warhead, materials of the target and the materials of the air domain:
- the case of warhead is made of Aluminium,
- the booster charge is from PETN 1.77,
- the explosive A-IX-I is used for main charge,
- the liner is from CuOF-HC,

- the new material properties have been added for wave shaper.

Two kinds of armour steel were used for the target formation: Armox 440T and S235JR. Compositions and basic properties of Armox 440T were obtained from [14] and S235JR from [15].

Some parts used the material parameters taken from the ANSYS AUTODYN library and the remaining parts used the material parameters obtained from the experiments or from FEM, Inc. Tabs 1-5 introduce the properties of chosen materials.
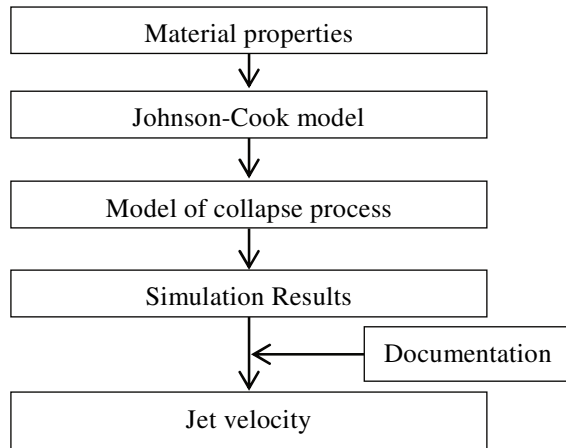
```
┌─────────────────────────┐
│   Material properties    │
└────────────┬────────────┘
             ↓
┌─────────────────────────┐
│   Johnson-Cook model     │
└────────────┬────────────┘
             ↓
┌─────────────────────────┐
│ Model of collapse process│
└────────────┬────────────┘
             ↓
┌─────────────────────────┐
│    Simulation Results    │←────┐
└────────────┬────────────┘     │
             ↓            ┌──────────────┐
┌─────────────────────────┐│ Documentation│
│       Jet velocity       │└──────────────┘
└─────────────────────────┘
```

Fig. 1 Diagram of jet formation process

```
┌──────────────────────────┐
│Material properties of target│
└─────────────┬────────────┘      ┌──────────────┐
              ↓              ┌─────│  Gap: 10 mm  │
┌──────────────────────────┐│     └──────────────┘
│    Johnson-Cook model     │←────┤
└─────────────┬────────────┘│     ┌──────────────┐
              ↓             └─────│  Gap: 20 mm  │
┌──────────────────────────┐      └──────────────┘
│     Penetration model     │
└─────────────┬────────────┘
              ↓
┌──────────────────────────┐      ┌──────────────┐
│     Simulation results    │←─────│  Experiment  │
└─────────────┬────────────┘      └──────────────┘
              ↓
┌──────────────────────────┐
│        Conclusion         │
└──────────────────────────┘
```
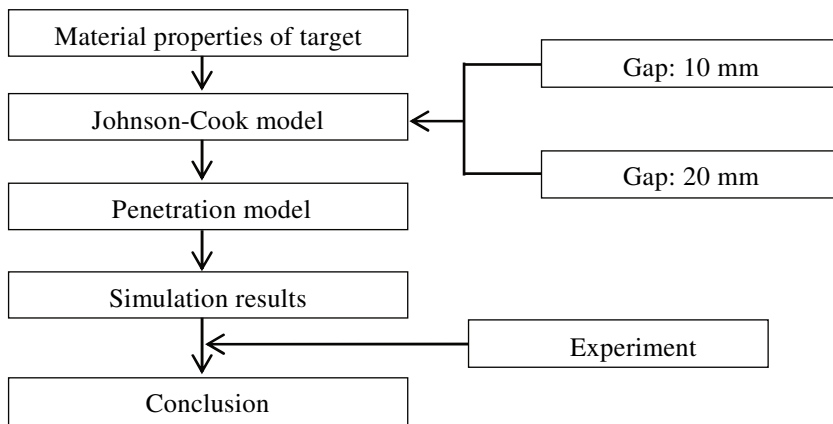
Fig. 2 Diagram of penetration simulation with gaps between plates of target

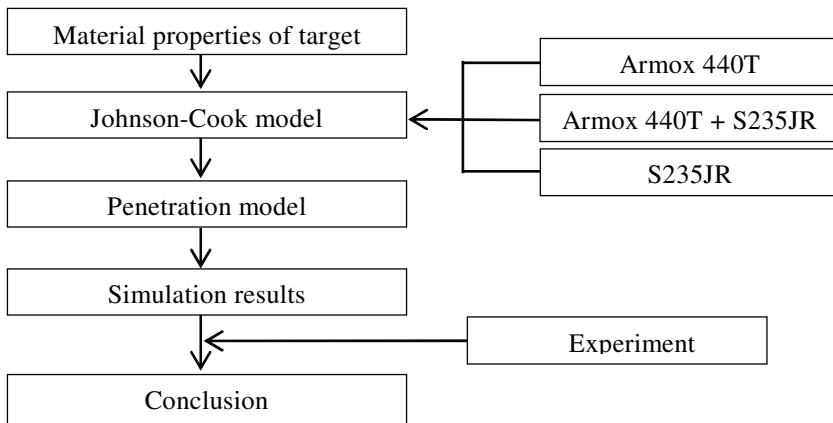*Fig. 3 Diagram of simulation in case of using targets with different materials*

Tab. 1 Properties of air

Name	Value	Unit
Density	1.225	kg m^{-3}
Equation of state	Ideal Gas	—
Specific heat ratio	1.4	—
Temperature	288	K
Specific heat capacity (v = const.)	0.7175999	kJ kg^{-1} K^{-1}
Initial internal energy	206.8	kJ kg^{-1}

Tab. 2 Material properties of booster and main charge

Name	Booster	Main charge	Unit
Density	1 770	1 700	kg m^{-3}
Equation of state	JWL	JWL	—
Parameter A	6.17×10^5	5.37167×10^5	MPa
Parameter B	1.69×10^4	5.37926×10^3	MPa
Parameter R1	4.4	4.2	—
Parameter R2	1.2	1	—
Parameter W	0.25	0.4	—
C-J detonation velocity	8 300	7 500	m s^{-1}
C-J energy	1×10^7	8×10^6	kJ m^{-3}
C-J pressure	3.35×10^4	2.9×10^4	MPa

Tab. 3 Material properties of case, liner and steel S235JR

Name	Case	Liner	S235JR	Unit
Density	2 770	8 930	7 896	kg m^{-3}
Equation of state	Shock	Shock	Shock	—
Gruneisen coefficient	2	1.99	2.17	—
Parameter C1	5.3×10^3	3.94	4.57×10^3	m s^{-1}
			Continued on the next page	

Name	Case	Liner	S235JR	Unit
Parameter S1	1.33	1.489	1.49	—
Strength model	Johnson-Cook	Johnson-Cook	Johnson-Cook	—
Shear modulus	2.76×10^4	4.7×10^4	8.18×10^4	MPa
Yield strength	337	89.7	350	MPa
Hardening constant	343	292	275	MPa
Hardening exponent	0.41	0.31	0.36	—
Strain rate constant	0.01	0.025	0.022	—

Tab. 4 Material properties of wave shaper

Name	Value	Unit
Density	1 385	$kg\ m^{-3}$
Equation of state	Shock	—
Gruneisen coefficient	1.3	—
Parameter C1	2.09×10^3	$m\ s^{-1}$
Parameter S1	1.35	—

Tab. 5 Material properties of Armox 440T

Name	Value	Unit
Density	7 830	$kg\ m^{-3}$
Equation of state	Linear	—
Bulk modulus	1.59×10^5	MPa
Reference temperature	300	K
Specific heat	0.477	$kJ\ kg^{-1}\ K^{-1}$
Strength model	Johnson-Cook	—
Shear modulus	7.7×10^4	MPa
Yield strength	1.11×10^3	MPa
Hardening constant	2×10^3	MPa
Hardening exponent	0.85	—
Strain rate constant	0.002	—
Thermal softening exponent	1.4	—
Failure model	Johnson-Cook	
Damage constant, D1	0.051	—
Damage constant, D2	0.82	—
Damage constant, D3	−0.46	—
Damage constant, D4	−0.04	—
Melting temperature	1 793	K

2.3. Experiment Setup

The experiments were carried out by the Military Research Institute in Brno at the Bzenec shooting range. The number of PG-7V warheads had been limited, therefore the experiments were carried out according to Tab. 6. The warhead was placed in an optimal standoff distance from the target 180 mm. The target was built from 17 pieces of Armox 440 plates (20 × 200 × 200) mm, which is shown in Fig. 4.

Fig. 5 shows the experimental setup when using target with air spaces between Armox 440T plates. The warhead is placed in an optimal standoff from the target. In these tests, the distances of gaps were 10 mm, resp. 20 mm. Fig. 6 shows the experimental setup when using S235JR target. The target is built from 24 pieces of S235JR plates $(20 \times 200 \times 200)$ mm.

Tab. 6 Overview of planned experiments for optimal standoff distance 180 mm

Experiment		Nº of tests
Armour material effect without gaps	Armox 440 T	3
	S235JR	2
	Armox 440T + S235JR	1
Gaps Effect (Armox 440T):	10 mm	2
	20 mm	2

Fig. 4 The test of Armox 440T target

Fig. 5 The target with air space between plates

3. Simulation of Target Characteristics Effect on Penetration Depth

The process of the jet formation simulated in the FEM model described the Eulerian grid created a high-speed jet. Then the jet was transferred to the Lagrangian grid with the same coordinate system as in case of the Eulerian grid and the target made of steel armour plates from the Armox 440T was built using the ALE grid. The types of grids used were consulted with the experts from ANSYS company. The materials properties of the jet and target are introduced in Tab. 4 and Tab. 5.

Fig. 6 The test of S235JR target

4. Simulation of Target Characteristics Effect on Penetration Depth

The process of the jet formation simulated in the FEM model described the Eulerian grid created a high-speed jet. Then the jet was transferred to the Lagrangian grid with the same coordinate system as in case of the Eulerian grid and the target made of steel armour plates from the Armox 440T was built using the ALE grid. The types of grids used were consulted with the experts from ANSYS company. The materials properties of the jet and target are introduced in Tab. 4 and Tab. 5.

4.1. Simulation Model of Jet Formation

Fig. 7 introduces the PG-7V model used for the jet formation simulation, which includes following parts: booster, case, wave shaper, main charge and liner.
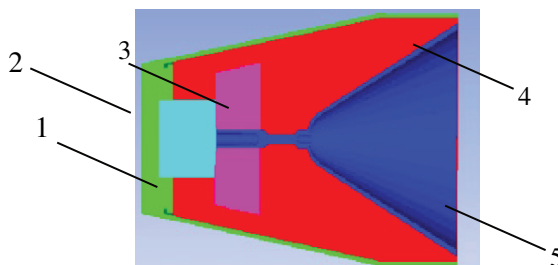
Fig. 7 Model of PG-7V warhead
1. booster; 2. case; 3. waveshaper; 4. main charge; 5. liner

In this model, the front part of the warhead was removed. All dimensions of the model were drawn according to the technical documentation of PG-7V warhead accessible on the Department of Weapons and Ammunition of University of Defence in Brno.

Using ANSYS AUTODYNE software, the FEM model was built up to determine the jet velocity, jet formation as well as the collapse process of the liner. All parts of the jet formation process model were described by an Eulerian grid. The model consists of 2 parts: PG-7V warhead and an air domain in front of it.

A coordinate system was built to determine positions of jet tip at any moment of jet moving. In this coordinate system, the $0x$ axis is axis of symmetry of the warhead, the rear edge of booster is chosen as $0y$ axis, and the origin is the intersection point of $0x$ and $0y$ axis. The coordinate system of the model was constructed as shown in

Fig. 8. Series of Gauss points were set on the $0x$ axis and the liner to obtain the jet tip velocity and other parameters. The detonation line was set at the rear edge of the booster. All parts were filled with materials presented in Tabs 1-4.
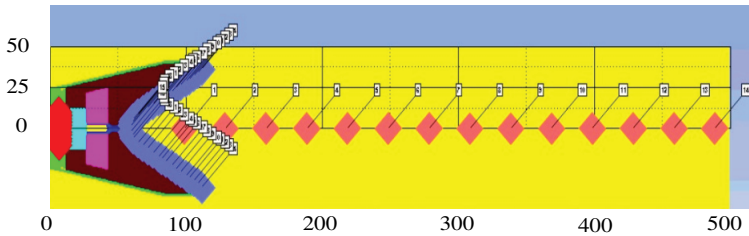

Fig. 8 FEM model of jet formation process

4.2. Jet Formation Simulation Results

All cases of simulation as well as experiments were performed when the warheads were located at the optimal standoff distance. According to technical documentation, the distance of the PG-7V warhead from the target to the rear edge of booster was between 318 mm and 332 mm, depending on the production precision of the warhead.

Based on the simulation results, Fig. 9 shows the graph of the velocity and the profile of the jet in the optimal stand-off distance position. At this moment, the coordinates of the jet tip are (327; 0).
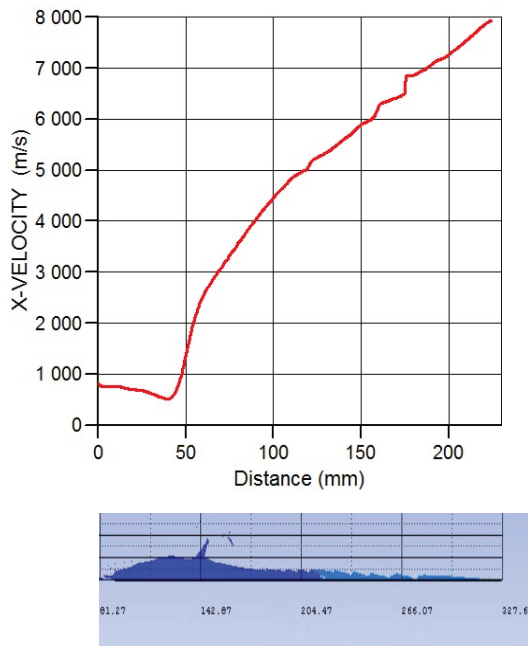
Fig. 9 Jet profile and jet velocity at optimal standoff distance

4.3. Influence of Gaps between Target Plates

Fig. 10 shows the formed jet of the modified PG-7V warhead and the target model with gaps 10 mm between the plates of the target. In the same way, Fig. 11 shows the jet – target models assembled in the case where gaps are 20 mm.
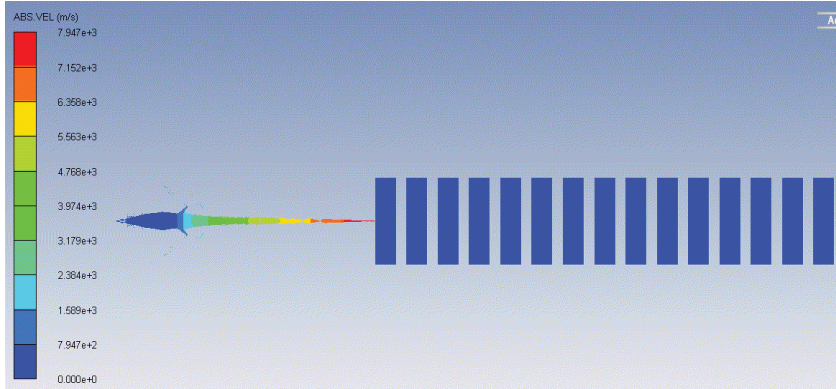
Fig. 10 Penetration model in case of 10 mm *gaps of target*
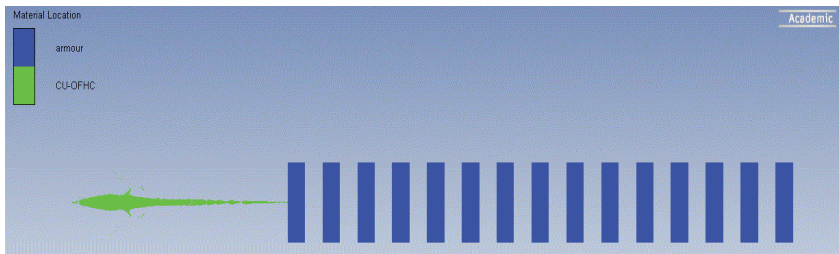
Fig. 11 Penetration model in case of 20 mm *gaps of target*

4.4. Effect of Target Materials Properties on Penetration Depth

The model of penetration jet into the target made of Armox 440T is shown in Fig. 12. Series of Gauss points were set on the $0x$ axis to obtain the jet tip velocity and the state of the target at any moment of simulation time.
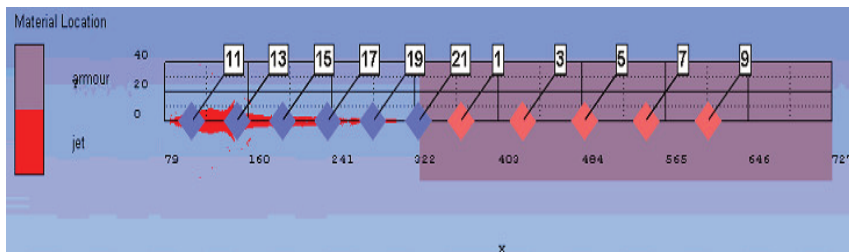
Fig. 12 Penetration model in case of Armox 440T target

In the same way, Fig. 13 shows the formed jet and target model at the optimal standoff distance at the moment of impact on the mixed target, which is formed alter-

nately of 20 mm Armox 440T armour plates and 20 mm S235JR plates. Material properties of Armox 440T were determined experimentally.
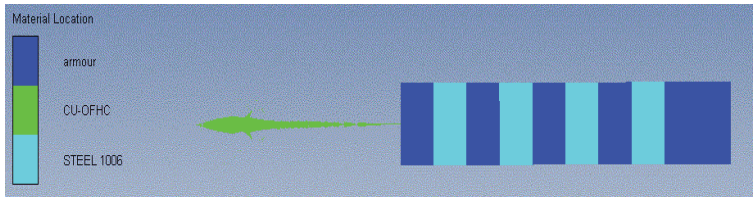
Fig. 13 Penetration model in case of mixed target

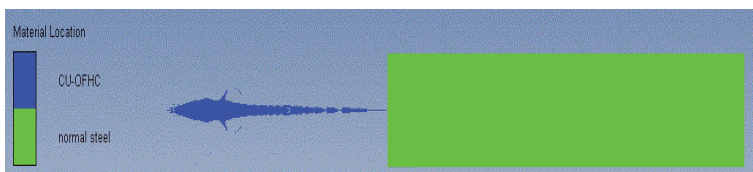Fig. 14 shows the model of penetration of the target formed by the material S235JR.

Fig. 14 Penetration model of the target from S235JR

5. Results and Discussion of Simulation and Experiments

5.1. Simulation of Air Spaces Effect between Plates of Target

The results indicate the state of the jet during the penetration process depending on time. Figs 15 and 16 show the state of jet – target system. The velocity of the jet depends on its length at 9.248×10^{-2} ms of simulation time. In this case, the gaps size is 10 mm.
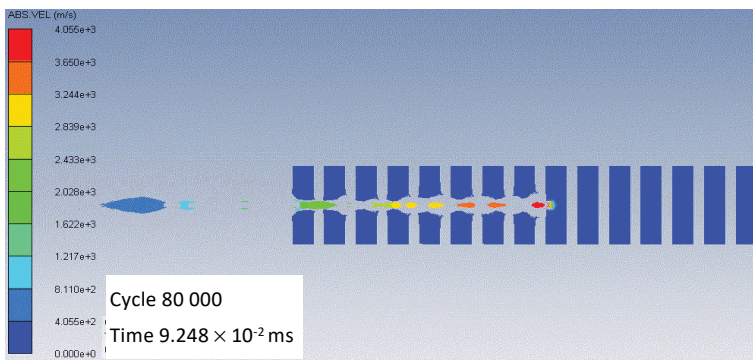
Fig. 15 Jet – target state of 9.248×10^{-2} ms *simulation time*

The dependence of the penetration depth on the selected gaps between the plates of the target is shown in Fig. 17. In case of the 20 mm or greater gaps, the penetration depths do not change significantly. According to the trend of the graph, when the gaps between the plates further increase, the penetration depth will be less affected.
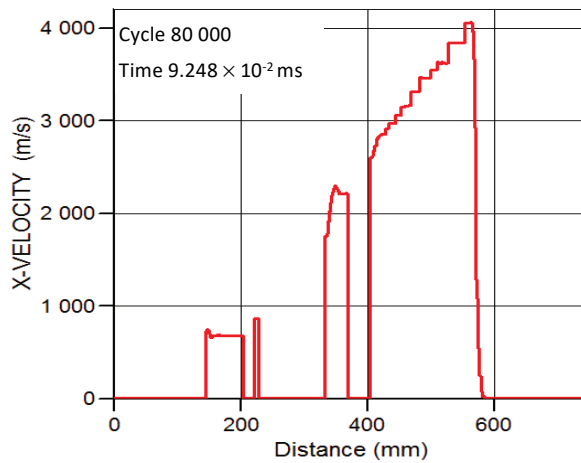
Fig. 16 Velocity of jet depending on its length at the time 9.248×10^{-2} ms

The dependence of the penetration depth on the selected gaps between the plates of the target is shown in Fig. 17. In case of the 20 mm or greater gaps, the penetration depths do not change significantly. According to the trend of the graph, when the gaps between the plates further increase, the penetration depth will be less affected.
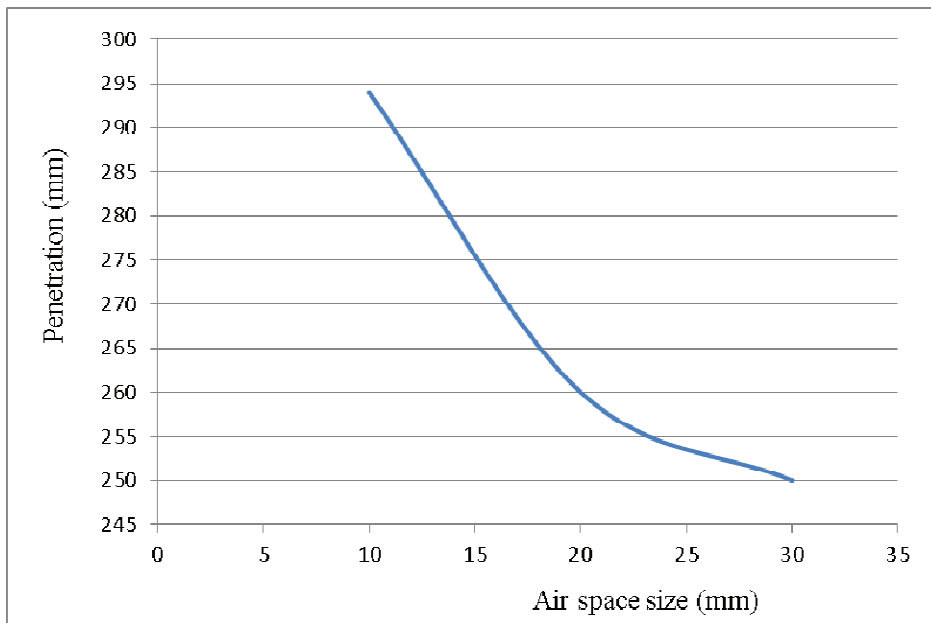
Fig. 17 Penetration depth depending on gap size of air space

Tab. 7 shows the comparison of the time and depth of penetration values in two cases. Obviously, the movement time of the slug does not depend on the gaps size between the target plates. In the case of penetration of plates with gaps, the jet has a greater velocity with larger gaps between plates of target.

Tab. 7 Comparison of the influence of gap sizes on penetration depths

Air space gap size	10 mm	20 mm
Time to separate the jet from the slug [ms]	1.933×10^{-2}	1.926×10^{-2}
The slug moves to the first plate [ms]	2.747×10^{-1}	2.697×10^{-1}
Time to stop the jet [ms]	3.626×10^{-1}	4.053×10^{-1}
Velocity of jet at the moment of separation from the slug [m s^{-1}]	6 805	6 810
Velocity of jet at the moment of the slug on the first plate [m s^{-1}]	2 230	2 316
Penetration depth [mm]	295	260

5.2. Simulation of Target Materials Properties Effect

Figs 18-20 compare the jet velocities at the different penetration depths in all three cases of the plate arrangement of the target.
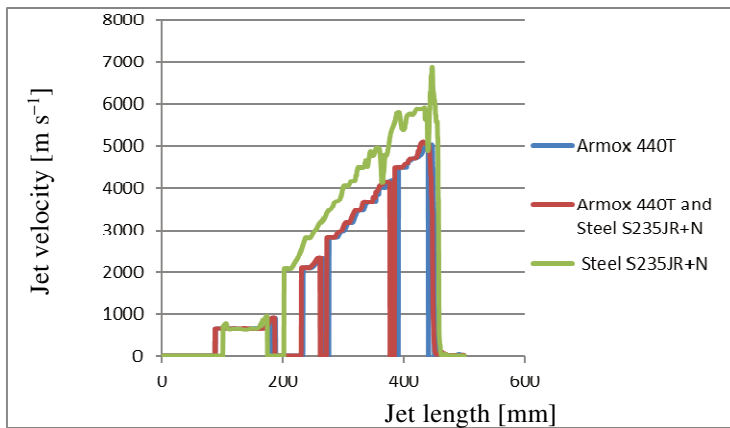

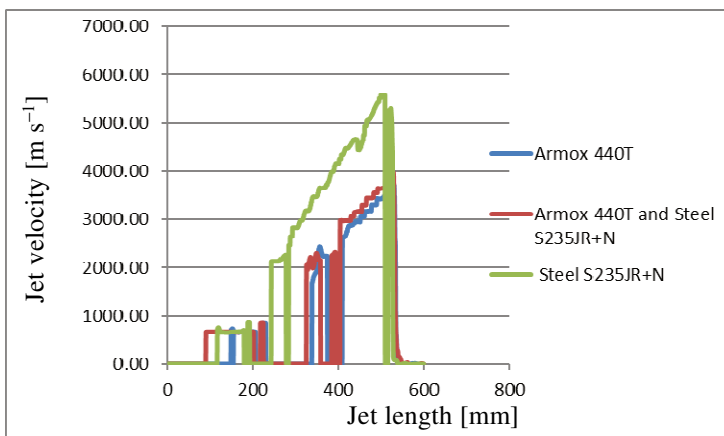*Fig. 18 Jet velocities depending on jet length at* 120 mm *penetration depth*

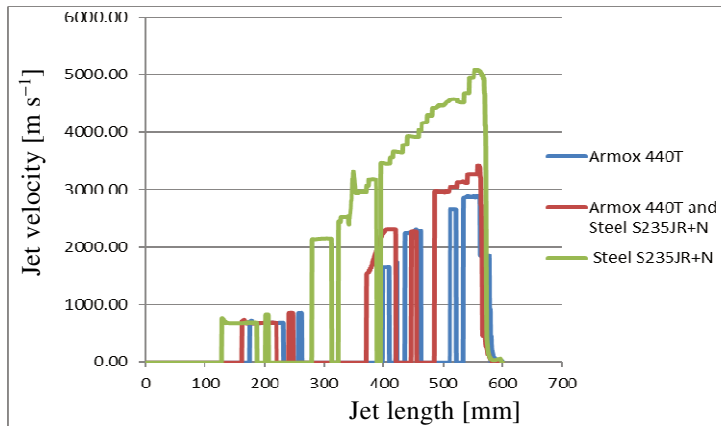*Fig. 19 Jet velocities depending on jet length at* 200 mm *penetration depth*

Fig. 20 Jet velocities depending on jet length at 240 mm *penetration depth*

At 120 mm penetration depth in the target formed by Armox 440T plates or the combination of Armox 440T and S235JR plates, the jet velocities and their structure are very similar. The jet tip velocity moving in the target formed by the Armox 440T and S235JR plate combination is 5 048 m s⁻¹. In case of the target composed only of Armox 440T plates, the jet tip velocity is 5 000 m s⁻¹ and 6 920 m s⁻¹ in case of the penetration into the S235JR plates.

The jet penetrating into the target composed of Armox 440T plates is divided into multiple sections (Figs 19 and 20). After the jet penetration at the depth of 200 mm into the S235JR plates, the jet tip velocity is 5 630 m s⁻¹. It is about 1.53 times greater than the jet tip velocity penetrating into the target from the Armox 440T plates and 1.41 times greater than the jet tip velocity penetrating into the target formed by Armox 440T and S235JR.

At 240 mm penetration depth in the S235JR plate target, the jet velocity is 5 160 m s⁻¹, which is 1.78 times greater than the jet tip velocity penetrating into the target from the Armox 440T plates and 1.49 times greater than the jet tip velocity penetrating into target from Armox 440T and S235JR plates.

Tab. 8 shows the comparison of time and the jet velocity simulation results depending on the penetration depth of three cases plate arrangement of the target.

Tab. 8 Comparison of time and jet tip velocities depending on the penetration depth

Target Depth	Armox 440T		Armox 440T + S235JR		S235JR	
	Time [ms]	Velocity [m s⁻¹]	Time [ms]	Velocity [m s⁻¹]	Time [ms]	Velocity [m s⁻¹]
120 mm	4.471×10^{-2}	5 000	4.324×10^{-2}	5 048	2.97×10^{-2}	6 920
200 mm	9.39×10^{-2}	3 682	8.69×10^{-2}	3 989	4.912×10^{-2}	5 630
240 mm	1.326×10^{-1}	2 893	1.144×10^{-1}	3 452	6.634×10^{-2}	5 160

Figs 21-23 show the results of the penetration simulation − penetration depth for all three variations of target.

It can be seen from Figs 21-23 that the penetration depth in the target from the S235JR plates is greater than 400 mm. It is about 1.35 times higher than the penetration depth in the target from the Armox 440T plates (305 mm) and 1.3 times higher than that one in the target composed from the Armox 440T and S235JR plates with a penetration depth value of 320 mm.
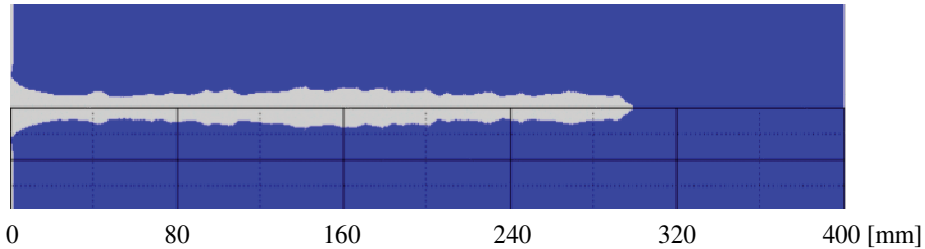

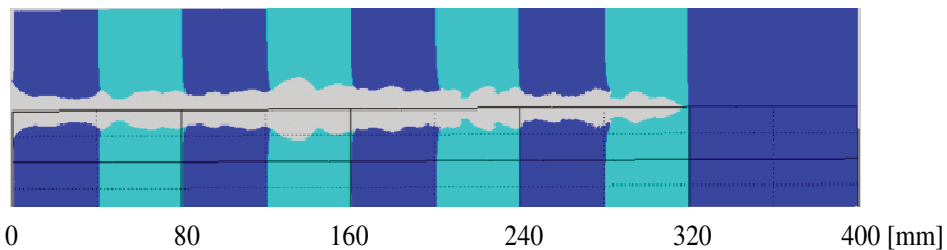*Fig. 21 The target composed of ARMOX 440T plates after penetration*

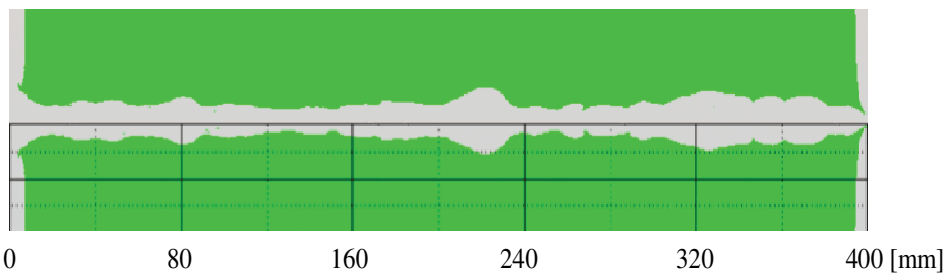*Fig. 22 The target composed of ARMOX 440T and S235JR plates after penetration*

Fig. 23 The target composed of S235JR plates after penetration

5.3. Comparison of Simulation and Experimental Results

The results of experiments carried out according to Tab. 6 and results of simulation are introduced in Tab. 9.

Comparing the penetration depth values in Tab. 9, the effect of the target material properties on the penetration depth is obvious. In case of penetration experiment using the S235JR plates, 20 plates were completely penetrated and the 21st plate was partially penetrated.

Tab. 9 Results of experiments

Type of test		Penetration depth [mm]	Simulation depth [mm]	Difference [%]
Armour mate- rial effect without gaps	Armox 440T	320, 305, 301	305	1.2
	S235JR	404, 405	410	1.3
	Armox 440T + S235JR	361	320	12.8
Gaps effect (Armox 440T)	10 mm	280, 305	295	0.3
	20 mm	270, 263	260	2.5

A comparison of the experimental results using the armour Armox 440T without gaps and using two different gaps is shown in Fig. 24. It is obvious that the penetration into the target decreases with larger gaps size of air space.

It is also obvious from Tab. 9 that the differences of the average experimental values and simulation results are not so high, i.e. in the range from 0.3% to 2.5%. In case of the composed target from two introduced steels, the difference is 12.8%.
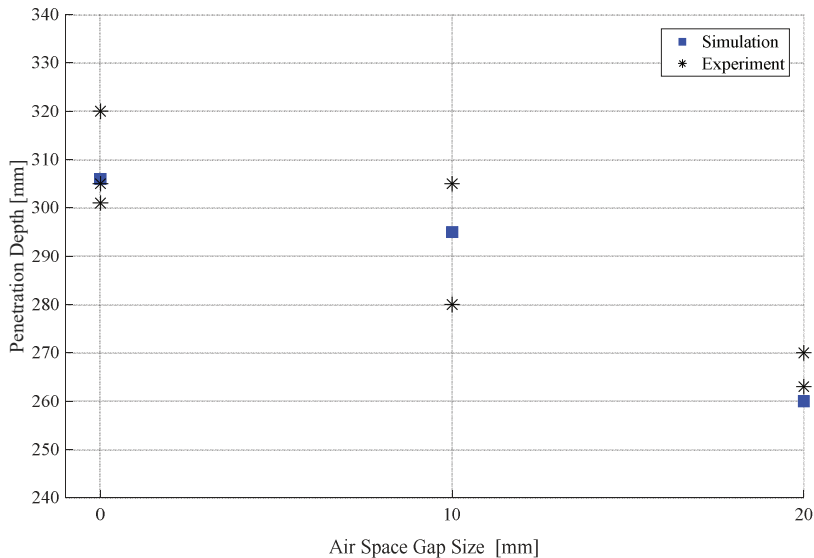

Fig. 24 Comparison of penetration depths at different gaps between plates obtained experimentally and by simulation

6. Conclusion

In this article, the 2D simulation model using ANSYS AUTODYN was built to observe/study the effect of the target materials properties as well as the gaps sizes between target plates on the penetration depth values.

Comparison of simulation and experimental results proves their very good correspondence with exception of the armour combination. Therefore, the ANSYS

AUTODYN use for the penetration simulation of the armours of various properties and structures is possible and expedient when required input armour characteristics are known. Of course, the simulation results verification by the higher number of experiments is necessary. In this case, the higher number of PG-7V warheads or another HEAT ammunition for experiments were not available.

Despite the small amount of experiments, significant conclusions have been proved. The penetration depth of the target composed of the armour plates is comparable with that one of homogenous ballistic protection introduced for this ammunition. The regular gaps between the armour plates decrease the penetration depth. In spite of that, the penetration of armoured vehicles is still sufficient.

References

[1]   SMOLIK, J. *Calculation and Construction of Shaped Charge* (in Czech). Brno: VAAZ, 1965. 95 p.

[2]   WALTERS, W.P and ZUKAS, J.A. *Fundamentals of Shaped Charges*. New York: Wiley, 1989. 398 p. ISBN 0-471-62172-2.

[3]   WANG, C., XU, W. and YUEN, S.C.K. Penetration of Shaped Charge into Layered and Spaced Concrete Targets. *International Journal of Impact Engineering*, 2018, vol. 112, p. 193-206. DOI 10.1016/j.ijimpeng.2017.10.013.

[4]   GUO, H., ZHENG, Y., YU, Q., GE, C.F. and WANG, H. Penetration Behaviour of Reactive Liner Shaped Charge Jet Impacting Thick Steel Plates. *International Journal of Impact Engineering*, 2019, vol. 126, p. 76-84. DOI 10.1016/j.ijimpeng.2018.12.005.

[5]   WANG, C., XU, W. and LI, T. Experimental and Numerical Studies on Penetration of Shaped Charge into Concrete and Pebble Layered Targets. *International Journal of Multiphasic*, 2017, vol. 11, no. 3, p. 295-314. DOI 10.21152/1750-9548.11.3.295.

[6]   MURPHY, M.J. *Development of a 71 mm Two-Stage Warhead.* (UCID-19651). Livermore (USA): Lawrence Livermore National Laboratory, 1982.

[7]   SIMON, J., DIPERSIO, R. and MERENDINO, A.B. *The Penetration Capability and Effectiveness of a Precision Shaped Charge Warhead*. (Memorandum Report No. 1636). Aberdeen: Ballistic Research Laboratory, 1965. AD #5249451.

[8]   DIPERSIO, R. and SIMON, J. *Theory of Residual Penetration by Ideal Shaped Charge Jets.* (Report No. 1313). Aberdeen: Ballistic Research Laboratory, 1966.

[9]   MERENDINO, A.B. and VITALI, R. *The Penetration of Shaped Charge Jets into Steel and Aluminium Targets of Various Strengths*. (Memorandum Report No. 1932). Aberdeen: Ballistic Research Laboratory, 1968.

[10] HELD, M. Characterizing Shaped Charge Performance by Stand-off Behaviour. In *Proceedings of the 7th International Symposium on Ballistics*. Haag: MBB GmbH, 1983. 10 p.

[11] DEHN, J.T. *A Unified Theory of Penetration*. (Technical Report BRL-TR-2770). Aberdeen: Ballistic Research Laboratory, 1986.

[12] FOSTER, J.S. Integrated Flash Radiograph Analysis – an Approach to Studying Time-Dependent Phenomena in the Explosive Formation and Projection of Met-

als. In *Proceedings of 7th Annual Technical Meeting on Physical Explosion.* Livermore: Lawrence Livermore National Laboratory, 1981.

[13] *ANSYS Autodyne User's Manual*. Canonsburg: Ansys Inc., 2017, 512 p.

[14] *Armox® 440T* [online]. [viewed 2020-02-11]. Available from: www.ssab.com/products/brands/armox/armox-440t

[15] *Plates Product Catalogue 2019* [online]. [viewed 2020-02-11]. Available from: www.vitkovicesteel.com/data/soubory/plechy/Katalog_plechy_A4_2018_cely_oprava1-40_2_tisk6_web.pdf